

# Convergence and Quantum Advantage of Trotterized MERA for Strongly-Correlated Systems

Qiang Miao<sup>1,2</sup> and Thomas Barthel<sup>1</sup>

<sup>1</sup>*Department of Physics, Duke University, Durham, North Carolina 27708, USA*

<sup>2</sup>*Duke Quantum Center, Duke University, Durham, North Carolina 27701, USA*

(Dated: March 12, 2023)

Strongly-correlated quantum many-body systems are difficult to study and simulate classically. Our recent work [arXiv:2108.13401] proposed a variational quantum eigensolver (VQE) based on the multiscale entanglement renormalization ansatz (MERA) with tensors constrained to certain Trotter circuits. Here, we extend the theoretical analysis, testing different initialization and convergence schemes, determining the scaling of computation costs for various critical spin models, and establishing a quantum advantage. For the Trotter circuits being composed of single-qubit and two-qubit rotations, it is experimentally advantageous to have small rotation angles. We find that the average angle amplitude can be reduced substantially with negligible effect on the energy accuracy. Benchmark simulations show that choosing TMERA tensors as brick-wall circuits or parallel random-pair circuits yields very similar energy accuracies.

## I. INTRODUCTION

Due to the quantum advantage [1, 2] for certain tasks, quantum computers are expected to lead to a revolution in information technology. While there has been enormous theoretical and experimental progress, quantum computation currently still faces a number of challenges, including the limited number of qubits, inevitable noise, and insufficient fidelity [3, 4]. The simulation of quantum matter is less demanding and, hence, a promising field of application for the current era of noisy intermediate-scale quantum (NISQ) devices [5–14]. Compared with classical simulation techniques, quantum simulation methods can have substantially lower time complexity and may, hence, lead to new insights on quantum many-body physics in the near future.

In Ref. [10] we proposed a resource-efficient and noise-resilient [15] variational quantum eigensolver (VQE) for the simulation of strongly-correlated quantum many-body systems. This VQE is based on the multi-scale entanglement renormalization ansatz (MERA) [16] and gradient-based optimization. A strength of tensor network state (TNS) [16–22] techniques such as MERA is that they are applicable for frustrated quantum magnets and strongly-correlated fermionic systems [23–27], where quantum Monte Carlo is hampered by the sign problem [28, 29]. Nevertheless, a limiting factor for classical TNS simulations is the high computational cost, especially for  $D \geq 2$  spatial dimensions. We aim to overcome this problem by combining MERA with the VQE approach. In order to allow for an efficient experimental implementation, the MERA disentanglers and isometries are chosen as circuits of two-qubit gates. We refer to the latter as Trotter gates, because they get closer and closer to the identity when increasing the number of gates per MERA tensor [10]. This construction leads to what we call Trotterized MERA (TMERA) [30]. Recently, the VQE approach has been applied to small quantum chemistry problems [31–38]. We expect that TMERA will lead to similar progress for quantum many-body problems, particularly for strongly-correlated systems which cannot be easily

simulated on classical computers.

This paper extends the analysis of Ref. [10]. Sec. IV describes and analyzes different schemes for initializing the TMERA optimization and driving it to convergence with the goal of avoiding local minima. Iteratively increasing the number of variational parameters can substantially improve the performance. One can also start from system parameters with a well-known low-entangled ground state and, during the optimization, then move on certain paths through the space of model parameters to obtain the actual ground state of interest. In Sec. V, we analyze the quantum computational complexity of TMERA and compare to the classical computation costs of full MERA, taking into account the stochastic nature of quantum measurements. We identify critical one-dimensional spin- $s$  quantum magnets, for which TMERA displays a polynomial quantum advantage over the classical method. In the considered examples, the quantum advantage increases with increasing spin quantum number  $s$ . Larger quantum advantages are expected for systems in  $D \geq 2$  spatial dimensions. Small two-qubit rotation angles are desirable for implementations on present-day devices. In Sec. VI, we add an angle penalty term to the energy functional and find that the average angle can be reduced considerably without substantially affecting energy accuracies. The initial TMERA proposal [10] chooses all MERA tensors as brick-wall circuits (a.k.a. alternating layered ansatz) with generic two-qubit gates acting on nearest neighbors. In Sec. VII, we replace the brick-wall circuits by parallel random-pair circuits (PRPC). While PRPC contain long-range two-qubit gates, they do not seem to outperform brick-wall circuits, as long as bond dimensions are small.

## II. TMERA AND TENSOR CIRCUIT STRUCTURE

Let us consider a lattice system with  $N$  sites, each associated with a single-site Hilbert space of dimension  $d$ . If a VQE completely replicates the physical system, the

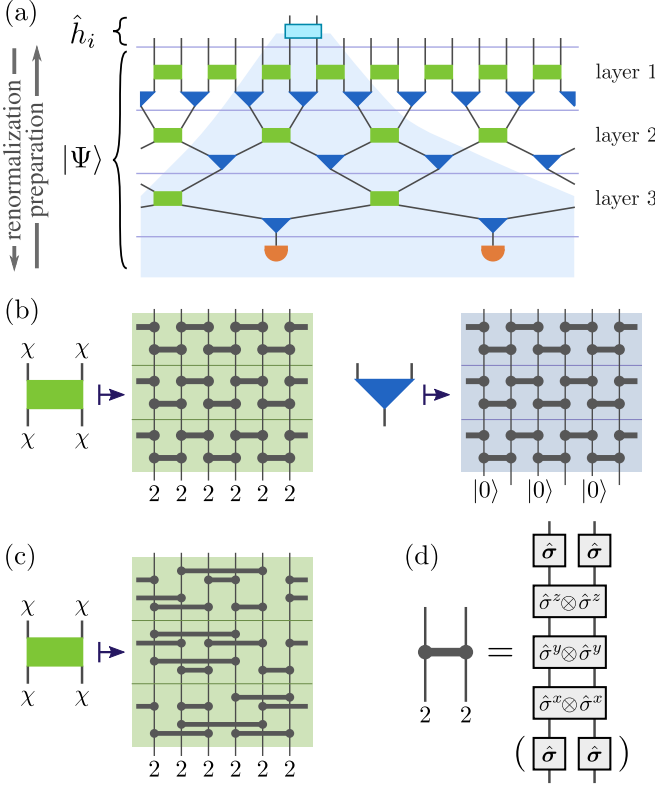


FIG. 1. **Circuit structures for Trotterized MERA.** (a) A binary MERA with  $T = 3$  layers. The shaded region indicates the causal cone of a two-site operator  $\hat{h}_i$ . In TMERA, all unitary disentanglers and isometries are chosen as Trotter circuits. Panel (b) shows a corresponding brick-wall circuit consisting of nearest-neighbor two-qubit gates with  $t = 3$  Trotter steps and bond dimension  $\chi = 2^3$ , i.e.,  $q = 3$  qubits per renormalized site. Panel (c) illustrates the alternative choice of a parallel random-pair circuit. (d) Each two-qubit gate can be realized by single-qubit and two-qubit rotations.

required number of qubits grows linearly in the system size  $N$ . This can be avoided by employing tensor network structures [6, 10, 12–14, 39, 40]. We consider MERA  $|\Psi\rangle$  as shown in Fig. 1 that are suitably adapted for VQE. The hierarchical structure of MERA is motivated by real-space renormalization group. In each layer  $\tau$ , degrees of freedom of the system are disentangled to some extent by unitaries before isometries reduce the total number of sites by a factor of  $b$  in the transition to layer  $\tau + 1$ ;  $b$  is called the branching ratio. After  $T \lesssim \log_b(N)$  layers the procedure is stopped by projecting each site onto a reference state. Seen in reverse, this procedure prepares a quantum state for the physical system.

The expectation value  $\langle \Psi | \hat{h}_i | \Psi \rangle$  of a local operator only depends on the MERA tensors in the causal cone of  $\hat{h}_i$ . As a result, at most  $\mathcal{O}(\log N)$  qubits are needed to evaluate energy expectation values and gradients. This is because only a small constant number of new qubits per layer is introduced in each layer transition  $\tau \rightarrow \tau - 1$  to realize the isometries. As the same number of qubits leaves

the causal cone in each layer transition, mid-circuit resets [41–45] can eliminate the  $N$  dependence completely [10]. The accuracy of MERA is controlled by the bond dimension  $\chi$  of the tensors (equal to the Hilbert-space dimension of each renormalized site) and the number  $T$  of layers. On the quantum computer, each renormalized site is represented by  $q$  qubits such that  $\chi = 2^q$ .

It is possible to implement this protocol for a full MERA on a quantum computer, but imposing an additional structure/constraint on the MERA tensors will greatly enhance the performance. Figure 1 illustrates the idea of TMERA: A Trotter structure is imposed on every disentangler and isometry of the MERA. In Fig. 1b, each tensor is chosen as a brick-wall circuit with  $t$  Trotter steps, which contain nearest-neighbor two-qubit unitary gates. As a result, the quantum circuits for the evaluation of energy expectation values and gradients will have depth  $\mathcal{O}(tT)$ . Figure 1c shows an alternative Trotter structure – a parallel random-pair circuit (PRPC) consisting of arbitrary-range two-qubit gates. Per Trotter step, the PRPC contains the same number of gates as in the brick-wall circuit, but the qubit-pairs are chosen randomly. In both cases, the universal two-qubit gates can be implemented by a sequence of single-qubit rotations and CNOTs or, equivalently, single and two-qubit rotations [46–48]; see Fig. 1d.

### III. MODELS

To benchmark TMERA, we simulate various models for one-dimensional quantum magnets. They are all critical and, hence, highly-entangled with the long-range physics described by 1+1 dimensional conformal field theory (CFT) [49, 50]. We employ periodic boundary conditions for a lattice of  $N$  sites, the groundstate energy per site in the thermodynamic limit ( $N \rightarrow \infty$ ) is denoted by  $e_{\text{gs}}^\infty$ , and  $c$  is the central charge of the CFT.

**Spin-1/2 models.** – The spin-1/2 XXZ chain [51–53]

$$\hat{H}_{\frac{1}{2}} = \sum_i (\hat{S}_i^x \hat{S}_{i+1}^x + \hat{S}_i^y \hat{S}_{i+1}^y + \Delta \hat{S}_i^z \hat{S}_{i+1}^z) \quad (1)$$

is Bethe-ansatz integrable [54, 55], where  $\Delta$  is an anisotropy parameter. There is a critical spin-liquid phase when  $|\Delta| \leq 1$ , and the long-range physics can be explained by the sine-Gordon quantum field theory, which is a CFT with central charge  $c = 1$ . For  $|\Delta| < 1$ , the groundstate energy density is [56, 57]

$$e_{\text{gs}}^\infty = \frac{\Delta}{4} - \int dx \frac{1 - \Delta^2}{2 \cosh(\pi x) [\cosh(2x \arccos \Delta) - \Delta]}.$$

At the Berezinskii-Kosterlitz-Thouless (BKT) phase transition point  $\Delta = 1$ , we recover the isotropic Heisenberg antiferromagnet (XXX chain)  $\hat{H}_{\frac{1}{2}} = \sum_i \hat{S}_i \cdot \hat{S}_{i+1}$  with  $e_{\text{gs}}^\infty = \frac{1}{4} - \ln 2$  [58].

**Spin-1 models.** – The bilinear-biquadratic (BLBQ) spin-1 chain [59–66]

$$\hat{H}_1 = \sum_i [\cos \vartheta (\hat{\mathbf{S}}_i \cdot \hat{\mathbf{S}}_{i+1}) + \sin \vartheta (\hat{\mathbf{S}}_i \cdot \hat{\mathbf{S}}_{i+1})^2] \quad (2)$$

has several interesting quantum phases for the ground state. At the Takhtajan-Babujan (TB) point,  $\vartheta = -\frac{\pi}{4}$ , the model is Bethe-ansatz integrable and critical with central charge  $c = \frac{3}{2}$  and groundstate energy density  $e_{\text{gs}}^\infty = -2\sqrt{2}$  [62–64]. As  $\vartheta$  increases, we pass through the gapped Haldane phase,  $-\pi/4 < \vartheta < \pi/4$ , followed by a critical phase for  $\pi/4 \leq \vartheta < \pi/2$ . At the SU(3)-symmetric Uimin-Lai-Sutherland (ULS) point,  $\vartheta = \frac{\pi}{4}$ , the system can be solved by the nested Bethe ansatz [59–61], is described by a CFT with central charge  $c = 2$ , and has groundstate energy density  $e_{\text{gs}}^\infty = -\frac{\sqrt{2}}{2}(\ln 3 + \frac{\pi}{3\sqrt{3}} - 2)$  [59].

**Spin-3/2 models.** – The bilinear-biquadratic-bicubic (BLBQBC) spin-3/2 chain

$$\hat{H}_{\frac{3}{2}} = \sum_i \left[ -\frac{1}{16} \hat{\mathbf{S}}_i \cdot \hat{\mathbf{S}}_{i+1} + \frac{1}{54} (\hat{\mathbf{S}}_i \cdot \hat{\mathbf{S}}_{i+1})^2 + \frac{1}{27} (\hat{\mathbf{S}}_i \cdot \hat{\mathbf{S}}_{i+1})^3 \right] \quad (3)$$

is also Bethe-ansatz integrable [62–64]. Similar to the BLBQ spin-1 model at the TB point, it is an integrable analog of the isotropic spin-1/2 Heisenberg antiferromagnet for spin-3/2. It has a central charge  $c = \frac{9}{5}$ , and a groundstate energy density of  $e_{\text{gs}}^\infty = -\ln 2 - \frac{1}{8}$  [67].

Lastly, we consider the spin-3/2 XXX chain,

$$\hat{H}'_{\frac{3}{2}} = \sum_i \hat{\mathbf{S}}_i \cdot \hat{\mathbf{S}}_{i+1}, \quad (4)$$

which has central charge  $c = 1$  [68–70] and groundstate energy density  $e_{\text{gs}}^\infty \approx -2.82833$  [70–72]. While this half-integer spin model has similar critical properties like the spin-1/2 XXX chain [68, 70, 73–76], it is non-integrable and features higher entanglement due to the larger spin quantum number [77, 78].

#### IV. INITIALIZATION AND CONVERGENCE SCHEMES

To find a global minimum in a nonlinear optimization problem is generally non-trivial. The variational energy minimization for a many-body system can easily converge to local minima. We try the following approaches to address this problem for the TMERA VQE:

- *Direct TMERA:* One may simply optimize the TMERA without modifications.
- *TTTN $\rightarrow$ TMERA:* It can be beneficial to begin with a reduced set of parameters and then gradually increase the complexity of the variational ansatz. Specifically, we may first remove all disentanglers (set them to  $\mathbb{1}$ ) such that the TMERA

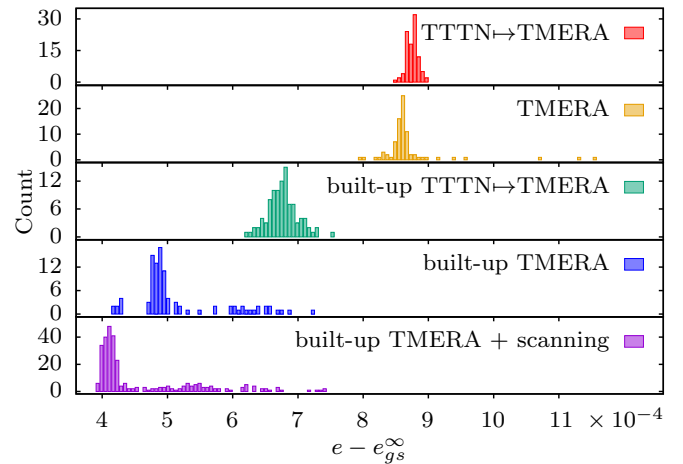


**FIG. 2. Convergence schemes.** The figure shows histograms of converged energy densities  $e$  for the spin-1/2 XXZ model (1) at  $\Delta = 1$  using homogeneous modified binary TMERA with  $T = 6$  layers,  $t = 8$  Trotter steps and bond dimension  $\chi = 8$  ( $q = 3$ ). From top to bottom, the convergence methods are: a) optimizing a TTTN with  $T = 6$ , and then switching to TMERA; b) directly optimizing a TMERA with  $T = 6$ ; c) building up a TTTN layer by layer and then switching to TMERA; d) building up a TMERA layer by layer; and e) building up a TMERA layer by layer at  $\Delta = 2$  and then scanning in the range  $\Delta \in [0, 2]$ .

becomes a Trotterized tree tensor network (TTTN) [79, 80]. The converged TTTN, is then used to initialize the TMERA.

- *Built-up TMERA:* A similar idea is to build up the TMERA tensor network layer by layer, i.e., iteratively increase the number of parameters during the optimization [81].
- *Scanning:* A powerful method is to start the optimization at a point in the phase space of the model, where we know the ground state very well or know, for example, that it is low-entangled such that it can easily be determined. In a “scanning” procedure, one then moves on suitable paths through the parameter space of the Hamiltonian during the optimization, until obtaining the actual ground state of interest.

One can also combine these ideas, e.g., by first building up a TTTN and then switching to TMERA.

In every scheme, we initialize all relevant tensors randomly at the beginning of the optimization procedure. Note that this could, in principle, lead to the barren-plateau phenomenon of exponentially small initial gradients [82, 83]. In Refs. [84, 85], we show that TMERA are not hampered by this problem. For tensors of the first layer ( $\tau = 1$ ), the average gradient of random tree tensor networks and MERA decreases polynomially with increasing bond dimension  $\chi$ . For higher layers, it decreases as  $(b\eta)^\tau$ , where  $\eta$  is the second largest eigenvalue

of a (doubled) layer transition channel, which is also polynomial in  $\chi$  [84, 85].

To test the performance of the different convergence methods, we run each a few hundred times, starting from different random initializations. Figure 2 shows results for the spin-1/2 XXZ chain with homogeneous modified binary TMERA using a Riemannian L-BFGS optimization [10, 86–88]. The resulting TMERA energy densities  $e$  are compared to the exact infinite-system value  $e_{\text{gs}}^\infty$ . While the  $e$  distributions for TTTN  $\mapsto$  TMERA and direct TMERA are narrow, without building up, their average and lowest  $e$  are considerably above  $e_{\text{gs}}^\infty$ . Our experience is that building up TMERA yields better performance than building up TTTN and then switching to TMERA. There are a few exceptions to this rule, e.g., for the BLBQ spin-1 chain at  $\vartheta = \pi/4$ . For the spin-1/2 XXZ chain, the scanning scheme gives somewhat better result than the built-up TMERA. Here, we started from the low-entangled ground state at  $\Delta = 2$  in the Néel phase and then scanned forth and back in the range  $0 \leq \Delta \leq 2$  until reaching convergence at  $\Delta = 1$ .

## V. COMPUTATIONAL COMPLEXITY

The computation time for evaluating the TMERA expectation value of a local interaction term  $\hat{h}_i$  on the quantum computer is proportional to the circuit depth  $\mathcal{O}(tT)$ . For the employed gradient-based optimization algorithm, we need to determine the gradient with respect to every Trotter gate (to a certain accuracy). As explained in Ref. [10], the total quantum computation time for a single measurement of all gradients is  $\mathcal{O}(q(tT)^2)$ . Of course, the quantum computer yields probabilistic digital outcomes rather than exact expectation values. Therefore, one has to consider the number of measurement samples  $N_s$  needed in each optimization step. The corresponding statistical error  $\epsilon$  improves with the number of measurement samples  $N_s$  as  $\epsilon \propto 1/\sqrt{N_s}$ . Hence, the quantum cost for each TMERA optimization step is  $\mathcal{O}(qt^2T^2/\epsilon^2)$ . Quantum amplitude estimation (QAE) [89, 90] can reduce the required number of samples from  $\mathcal{O}(1/\epsilon^2)$  to  $\mathcal{O}(\log(1/\epsilon))$  while increasing the circuit depth by a factor  $\mathcal{O}(1/\epsilon)$  [91]. Hence, the resulting quantum computation time scales as

$$\mathcal{O}\left(\frac{qt^2T^2}{\epsilon} \log \frac{1}{\epsilon}\right). \quad (5)$$

The computation time for (unconstrained) full MERA (fMERA) on classical computers follows a power law  $\mathcal{O}(\chi^r)$  with rather large exponents  $r$  especially in  $D \geq 2$  spatial dimensions. In particular,  $r = 7, 8, 9$  for modified binary MERA, ternary MERA, and binary MERA in  $D = 1$  dimension [92], and  $r = 16, 28$  for  $3 \times 3 \mapsto 1$  and  $2 \times 2 \mapsto 1$  MERA in  $D = 2$  dimensions [93, 94]. The attainable energy accuracy also follows a power law,  $e - e_{\text{gs}}^\infty = \mathcal{O}(\chi^{-\beta})$  [92]. To compare the time complexities of TMERA VQE and classical fMERA computations, we

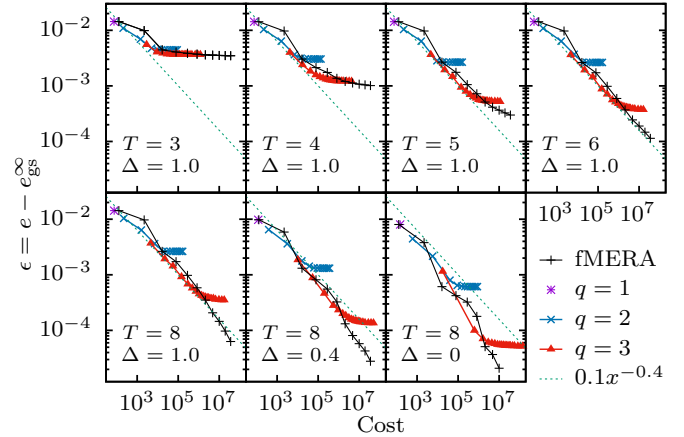


FIG. 3. Comparison of classical and VQE time complexities for critical spin-1/2 XXZ chains. The energy accuracy  $\epsilon = e - e_{\text{gs}}^\infty$  is shown as a function of the total computation time per iteration. For the latter, we use  $\chi^7$  for classical fMERA simulations and  $qt^2 \log(\frac{1}{\epsilon})/\epsilon$  for the TMERA VQE. For  $\Delta = 1$  and different numbers of layers  $T$ , the top panels show saturation effects when varying  $t$  for TMERA and  $\chi$  for fMERA. For the lower panels,  $T = 8$  is fixed and the anisotropy parameter  $\Delta$  of the model (1) is varied. The dashed line indicates the estimated accuracy-cost scaling of TMERA for the spin-1/2 XXX model ( $\Delta = 1$ ). We use homogeneous modified binary MERA and the scanning method. The data points, show the minimum of the energy density from a few hundred randomly initialized optimizations. We use fMERA with  $\chi \leq 12$ , and TMERA with  $t \leq 6$  for  $q = 2$ , and  $t \leq 16$  for  $q = 3$ .

can simply set  $\epsilon = e - e_{\text{gs}}^\infty$  since the attainable energy accuracy is intimately related to the statistical error of energy gradients. Thus, the classical cost is  $\mathcal{O}(\epsilon^{-r/\beta})$ .

For various critical spin models, the computation costs per iteration as a function of the energy accuracy  $e - e_{\text{gs}}^\infty$  are shown in Figs. 3 and 4, and discussed in the following. The numerical results confirm that the energy accuracy follows power laws for both TMERA and fMERA if the number of layers  $T$  is sufficiently large.

### A. Saturation with respect to $t$ and $\chi$

When increasing the number of Trotter steps  $t$  while  $q$  is fixed, the TMERA accuracy improves until reaching the fMERA accuracy for bond dimension  $\chi = 2^q$ . It is preferable to avoid this saturation regime and, instead, increase  $q$  beforehand [10].

The attainable accuracy also depends on the number of layers  $T$ . For the considered critical models and fixed  $T$ , the accuracy will saturate as a function of  $\chi$ . This is due to the infinite correlation length in these systems, where the long-range correlations of the targeted ground states can only be encoded in higher-layer tensors. The top panels in Fig. 3 clearly demonstrate this saturation for TMERA and fMERA. For the spin-1/2 XXZ model

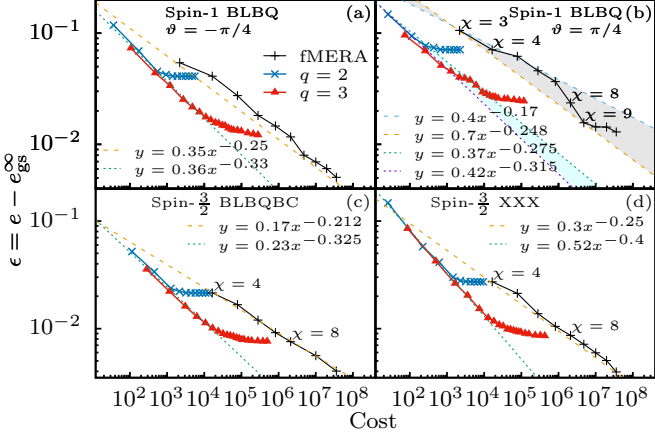


FIG. 4. Comparison of classical and VQE time complexities for critical spin-1 and 3/2 chains. As in Fig. 3, the energy accuracy is shown as a function of the total computation time per iteration. We use homogeneous modified binary MERA with  $T = 6$  layers, which is sufficient for the considered models (2), (3), and (4). The MERA are built-up. For the BLBQ model at  $\vartheta = \pi/4$ , the built-up TTN  $\rightarrow$  MERA method and scanning are also used. Each data point represents the minimum of the energy density from a few hundred randomly initialized optimizations. We use  $\chi \leq 12$  and, in TMERA,  $t \leq 6$  for  $q = 2$ , and  $t \leq 16$  for  $q = 3$ .

(1) at  $\Delta = 1$ , the numerical results suggest that  $T = 6$  layers are sufficient for  $\chi \leq 8$  and  $T = 8$  for  $\chi \leq 12$ . For smaller  $\Delta \in [0, 1)$ , one needs to increase the number of layers further to avoid the saturation. This may be attributed to the fact that the decay of the transverse correlation function  $|\langle \hat{S}_i^x \hat{S}_j^x \rangle| \sim |i - j|^{-\eta}$  is slower for smaller  $\Delta$ , where the critical exponent is given by

$$\eta = 1 - \arccos(\Delta)/\pi \in [1/2, 1]. \quad (6)$$

The longitudinal correlations always decay faster with  $|\langle \hat{S}_i^z \hat{S}_j^z \rangle| \sim |i - j|^{-1/\eta}$  [53, 95]. For the higher-spin models, we find that  $T = 6$  layers are sufficient when  $\chi \leq 12$ ; see Fig. 4.

## B. Quantum advantage

Choosing a sufficiently large number of layers  $T$ , we can now determine the scaling of the achievable accuracies for classical fMERA computations and the TMERA VQE as a function of the computational complexity. The bottom panels in Fig. 3 show corresponding data for the spin-1/2 XXZ chain (1) with  $\Delta = 1, 0.4$ , and 0. For this model, TMERA and fMERA display a rather similar scaling with the performance of both improving with decreasing  $\Delta$ . While the  $\langle \hat{S}_i^x \hat{S}_j^x \rangle$  correlations decay slower and the central charge of the system is  $c = 1$  in the entire critical phase, the groundstate entanglement entropy decreases with decreasing  $\Delta$  [96].

Figure 4 shows the scaling analysis for the critical spin-1 and spin-3/2 systems. The numerical results demon-

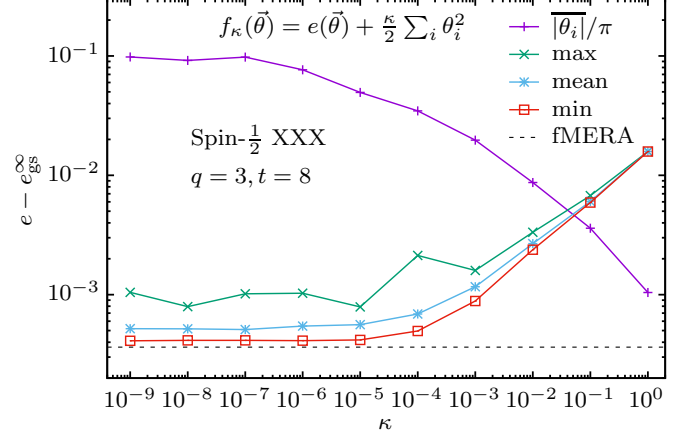


FIG. 5. Effect of large-angle penalties. The plot shows results for the spin-1/2 XXX model using homogeneous modified binary TMERA with  $T = 6$ ,  $t = 8$ , and  $q = 3$ . The modified objective function (9) comprises the energy density and a term penalizing large rotation angles. The three lower curves show the maximum, mean value, and minimum of energy density accuracy for a few hundred randomly initialized TMERA optimizations. The displayed average two-qubit rotation angle is obtained from the converged lowest-energy TMERA.

strate a polynomial quantum advantage of the TMERA VQE over the classical method for all considered models.

The spin-3/2 XXX chain (4) has the same central charge as its spin-1/2 counterpart, and the TMERA accuracy has almost the same scaling for both models. Interestingly, the fMERA shows a considerably worse scaling for the spin-3/2 case. This might be due to the increased number of local degrees of freedom, but further investigation is needed.

## VI. REDUCING ROTATION ANGLE AMPLITUDES

For experimental realizations, the TMERA Trotter gates are ultimately parametrized by rotation angles  $\theta$ , e.g., through the canonical decomposition for an arbitrary SU(4) matrix into single-qubit rotations like

$$\hat{R}_{\hat{\sigma}}(\alpha, \beta, \gamma) = e^{-i\alpha\hat{\sigma}^z/2} e^{-i\beta\hat{\sigma}^y/2} e^{-i\gamma\hat{\sigma}^z/2} \quad (7)$$

and two-qubit rotations

$$\hat{R}_{\hat{\sigma}^x \otimes \hat{\sigma}^x}(\theta) = e^{-i\theta\hat{\sigma}^x \otimes \hat{\sigma}^x/2}, \quad (8)$$

$\hat{R}_{\hat{\sigma}^y \otimes \hat{\sigma}^y}(\theta)$ , and  $\hat{R}_{\hat{\sigma}^z \otimes \hat{\sigma}^z}(\theta)$ ; see Fig. 1d and Refs. [47, 48]. With each gate corresponding to a unitary time evolution, the amplitudes of these angles determine the experimental simulation times or the intensities of manipulation pulses. Small rotation angles are desirable since both long evolution times and high pulse intensities decrease the quantum gate fidelity. We propose to reduce average rotation angle amplitudes by adding an angle

penalty term to the energy functional. Figure 5 shows optimization results for the modified objective function

$$f_\kappa(\boldsymbol{\theta}) = e(\boldsymbol{\theta}) + \frac{\kappa}{2} \sum_i \theta_i^2, \quad (9)$$

where the sum in the penalty term runs over the angles  $\{\theta_i\}$  of all two-qubit rotations. As expected, the average angle amplitude  $|\theta_i|$  decreases as the penalty parameter  $\kappa$  increases. We find that the average angle can be reduced by a factor of around 2 with negligible effect on the energy accuracy.

For data in Fig. 5, we used built-up TMERA and Euclidean L-BFGS, operating directly on the angles  $\boldsymbol{\theta}$ , instead of Riemannian L-BFGS. Alternatively, one could change the large-angle penalty term in Eq. (9) to  $\frac{\kappa}{2} \sum_j \|\hat{U}_j - \mathbb{1}\|^2$  with the sum running over all Trotter gates  $\hat{U}_j$  of the TMERA and, then, employ the Riemannian optimization as described in Ref. [10].

## VII. RANDOM CIRCUIT TMERA TENSORS

So far, we chose the TMERA tensors as brick-wall circuits with Trotter gates acting on nearest-neighbor qubits. The expressiveness and efficiency of the ansatz might be improved for alternative choices. In ion-trap systems one could, for example, use the all-to-all connectivity [97, 98] and work, instead, with parallel random-pair circuits (PRPC) as illustrated in Fig. 1c. Each Trotter step consists again of two Trotter-gate coverings. In each covering,  $n/2$  two-qubit gates act on disjoint qubit pairs, randomly chosen from the  $n$ -qubit support of the TMERA tensor. For the spin-1/2 Heisenberg antiferromagnet, Fig. 6 shows a comparison of TMERA accuracies for brick-wall circuit tensors and PRPC tensors. Even though a PRPC contains long-range two-qubit gates and hence allows a faster scrambling, the scaling of the attained accuracies is very similar, at least for this model and relatively small bond dimensions.

## VIII. DISCUSSION

For various critical spin systems in one spatial dimension, we have numerically confirmed that the TMERA VQE offers a polynomial quantum advantage over the classical fMERA simulations. The classical simulation cost jumps substantially from  $\mathcal{O}(\chi^{7\ldots 9})$  for one-dimensional systems [92] to  $\mathcal{O}(\chi^{16\ldots 28})$  for two-dimensional systems [93, 94]. This is due to the classically much more costly tensor contractions. As these are not relevant for the time complexity of the TMERA VQE, we expect that the quantum advantage will be much bigger in  $D = 2$  spatial dimensions. Unfortunately, it is currently not possible to properly determine the scaling of fMERA and TMERA costs and accuracies

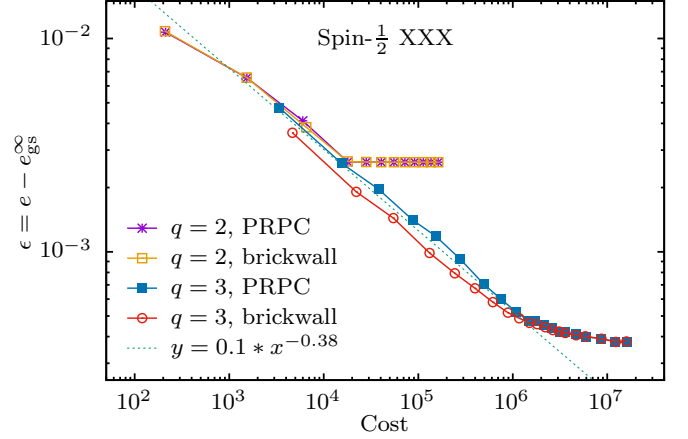


FIG. 6. **Energy accuracies for TMERA with brick-wall and PRPC tensors.** The plot shows the energy accuracy for the spin-1/2 Heisenberg antiferromagnet using homogeneous modified binary TMERA with two different circuit structures for the TMERA tensors,  $T = 6$  layers,  $t \leq 6$  Trotter steps for  $q = 2$ , and  $t \leq 16$  for  $q = 3$ . For each data point, we chose the minimum energy from a few hundred randomly initialized optimizations.

in classical simulations for  $D = 2$ . Experimental realization of the TMERA VQE should allow us to study two-dimensional systems.

Different circuit structures for the TMERA tensors produced very similar results, but were both composed of two-qubit gates. It would be interesting to explore whether multi-qubit gates, naturally available on different quantum computing platforms, improve the efficiency of the ansatz.

We found that the convergence can be improved substantially by gradually increasing the number of variational parameters and scanning in the model parameter space. One could explore further optimization methods like basin hopping [99] and quantum natural gradient [100, 101].

The success of the TMERA optimization for large quantum systems with substantial groundstate entanglement indicates that it is not hampered by barren plateaus. The absence of barren plateaus [82, 83] for isometric tensor network states, including matrix product states (MPS), tree tensor networks (TTN), MERA and TMERA, is shown rigorously in [84, 85].

## ACKNOWLEDGMENTS

We gratefully acknowledge helpful discussions with Marko Cetina, Kenneth R. Brown, and Yikang Zhang, and support through US Department of Energy grant DE-SC0019449.

---

[1] F. Arute, K. Arya, R. Babbush, D. Bacon, J. C. Bardin, R. Barends, R. Biswas, S. Boixo, F. G. Brandao, D. A. Buell, *et al.*, *Quantum supremacy using a programmable superconducting processor*, *Nature* **574**, 505 (2019).

[2] H.-S. Zhong, H. Wang, Y.-H. Deng, M.-C. Chen, L.-C. Peng, Y.-H. Luo, J. Qin, D. Wu, X. Ding, Y. Hu, *et al.*, *Quantum computational advantage using photons*, *Science* **370**, 1460 (2020).

[3] K. Bharti, A. Cervera-Lierta, T. H. Kyaw, T. Haug, S. Alperin-Lea, A. Anand, M. Degroote, H. Heimonen, J. S. Kottmann, T. Menke, W.-K. Mok, S. Sim, L.-C. Kwek, and A. Aspuru-Guzik, *Noisy intermediate-scale quantum algorithms*, *Rev. Mod. Phys.* **94**, 015004 (2022).

[4] D. Stilck França and R. Garcia-Patron, *Limitations of optimization algorithms on noisy quantum devices*, *Nat. Phys.* **17**, 1221 (2021).

[5] D. Wecker, M. B. Hastings, N. Wiebe, B. K. Clark, C. Nayak, and M. Troyer, *Solving strongly correlated electron models on a quantum computer*, *Phys. Rev. A* **92**, 062318 (2015).

[6] J.-G. Liu, Y.-H. Zhang, Y. Wan, and L. Wang, *Variational quantum eigensolver with fewer qubits*, *Phys. Rev. Research* **1**, 023025 (2019).

[7] A. Smith, M. Kim, F. Pollmann, and J. Knolle, *Simulating quantum many-body dynamics on a current digital quantum computer*, *npj Quantum Inf.* **5**, 106 (2019).

[8] M. Motta, C. Sun, A. T. Tan, M. J. O'Rourke, E. Ye, A. J. Minnich, F. G. Brandão, and G. K. Chan, *Determining eigenstates and thermal states on a quantum computer using quantum imaginary time evolution*, *Nat. Phys.* **16**, 205 (2020).

[9] C. Cade, L. Mineh, A. Montanaro, and S. Stanisic, *Strategies for solving the Fermi-Hubbard model on near-term quantum computers*, *Phys. Rev. B* **102**, 235122 (2020).

[10] Q. Miao and T. Barthel, *A quantum-classical eigensolver using multiscale entanglement renormalization*, *arXiv:2108.13401* (2021).

[11] F. Barratt, J. Dborin, M. Bal, V. Stojovic, F. Pollmann, and A. G. Green, *Parallel quantum simulation of large systems on small NISQ computers*, *npj Quantum Inf.* **7**, (2021).

[12] M. Foss-Feig, D. Hayes, J. M. Dreiling, C. Figgatt, J. P. Gaebler, S. A. Moses, J. M. Pino, and A. C. Potter, *Holographic quantum algorithms for simulating correlated spin systems*, *Phys. Rev. Research* **3**, 033002 (2021).

[13] D. Niu, R. Haghshenas, Y. Zhang, M. Foss-Feig, G. K.-L. Chan, and A. C. Potter, *Holographic simulation of correlated electrons on a trapped-ion quantum processor*, *PRX Quantum* **3**, 030317 (2022).

[14] E. Chertkov, J. Bohnet, D. Francois, J. Gaebler, D. Gresh, A. Hankin, K. Lee, D. Hayes, B. Neyenhuis, R. Stutz, *et al.*, *Holographic dynamics simulations with a trapped-ion quantum computer*, *Nat. Phys.* **18**, 1074 (2022).

[15] I. H. Kim and B. Swingle, *Robust entanglement renormalization on a noisy quantum computer*, *arXiv:1711.07500* (2017).

[16] G. Vidal, *Entanglement renormalization*, *Phys. Rev. Lett.* **99**, 220405 (2007).

[17] R. J. Baxter, *Dimers on a rectangular lattice*, *J. Math. Phys.* **9**, 650 (1968).

[18] S. R. White, *Density matrix formulation for quantum renormalization groups*, *Phys. Rev. Lett.* **69**, 2863 (1992).

[19] H. Niggemann, A. Klümper, and J. Zittartz, *Quantum phase transition in spin-3/2 systems on the hexagonal lattice - optimum ground state approach*, *Z. Phys. B* **104**, 103 (1997).

[20] F. Verstraete and J. I. Cirac, *Renormalization algorithms for quantum-many body systems in two and higher dimensions*, *arXiv:cond-mat/0407066* (2004).

[21] U. Schollwöck, *The density-matrix renormalization group in the age of matrix product states*, *Ann. Phys.* **326**, 96 (2011).

[22] R. Orús, *A practical introduction to tensor networks: Matrix product states and projected entangled pair states*, *Ann. Phys.* **349**, 117 (2014).

[23] T. Barthel, C. Pineda, and J. Eisert, *Contraction of fermionic operator circuits and the simulation of strongly correlated fermions*, *Phys. Rev. A* **80**, 042333 (2009).

[24] P. Corboz and G. Vidal, *Fermionic multiscale entanglement renormalization ansatz*, *Phys. Rev. B* **80**, 165129 (2009).

[25] C. V. Kraus, N. Schuch, F. Verstraete, and J. I. Cirac, *Fermionic projected entangled pair states*, *Phys. Rev. A* **81**, 052338 (2010).

[26] P. Corboz, G. Evenbly, F. Verstraete, and G. Vidal, *Simulation of interacting fermions with entanglement renormalization*, *Phys. Rev. A* **81**, 010303(R) (2010).

[27] C. Pineda, T. Barthel, and J. Eisert, *Unitary circuits for strongly correlated fermions*, *Phys. Rev. A* **81**, 050303(R) (2010).

[28] E. Y. Loh, J. E. Gubernatis, R. T. Scalettar, S. R. White, D. J. Scalapino, and R. L. Sugar, *Sign problem in the numerical simulation of many-electron systems*, *Phys. Rev. B* **41**, 9301 (1990).

[29] M. Troyer and U.-J. Wiese, *Computational complexity and fundamental limitations to fermionic quantum Monte Carlo simulations*, *Phys. Rev. Lett.* **94**, 170201 (2005).

[30] A similar structure, which is called brick-wall qMERA, was proposed simultaneously in Ref. [102]. In their work, the expressiveness of quantum circuits was studied numerically on a binary qMERA with  $N = 32$  sites and  $T = 4$  layers. We focus on establishing a quantum advantage in terms of the TMERA computation cost using large systems with  $N \geq 128$ .

[31] P. J. O'Malley, R. Babbush, I. D. Kivlichan, J. Romero, J. R. McClean, R. Barends, J. Kelly, P. Roushan, A. Tranter, N. Ding, *et al.*, *Scalable quantum simulation of molecular energies*, *Phys. Rev. X* **6**, 031007 (2016).

[32] A. Kandala, A. Mezzacapo, K. Temme, M. Takita, M. Brink, J. M. Chow, and J. M. Gambetta, *Hardware-efficient variational quantum eigensolver for small molecules and quantum magnets*, *Nature* **549**, 242 (2017).

[33] J. I. Colless, V. V. Ramasesh, D. Dahmen, M. S. Blok, M. E. Kimchi-Schwartz, J. R. McClean, J. Carter, W. A.

de Jong, and I. Siddiqi, *Computation of molecular spectra on a quantum processor with an error-resilient algorithm*, *Phys. Rev. X* **8**, 011021 (2018).

[34] C. Hempel, C. Maier, J. Romero, J. McClean, T. Monz, H. Shen, P. Jurcevic, B. P. Lanyon, P. Love, R. Babbush, *et al.*, *Quantum chemistry calculations on a trapped-ion quantum simulator*, *Phys. Rev. X* **8**, 031022 (2018).

[35] S. McArdle, T. Jones, S. Endo, Y. Li, S. C. Benjamin, and X. Yuan, *Variational ansatz-based quantum simulation of imaginary time evolution*, *npj Quantum Inf.* **5**, 75 (2019).

[36] H. R. Grimsley, S. E. Economou, E. Barnes, and N. J. Mayhall, *An adaptive variational algorithm for exact molecular simulations on a quantum computer*, *Nat. Commun.* **10**, 3007 (2019).

[37] Y. Nam, J.-S. Chen, N. C. Pisenti, K. Wright, C. Delaney, D. Maslov, K. R. Brown, S. Allen, J. M. Amini, J. Apisdorf, *et al.*, *Ground-state energy estimation of the water molecule on a trapped-ion quantum computer*, *npj Quantum Inf.* **6**, 33 (2020).

[38] C. N. Self, K. E. Khosla, A. W. Smith, F. Sauvage, P. D. Haynes, J. Knolle, F. Mintert, and M. Kim, *Variational quantum algorithm with information sharing*, *npj Quantum Inf.* **7**, 116 (2021).

[39] W. Huggins, P. Patil, B. Mitchell, K. B. Whaley, and E. M. Stoudenmire, *Towards quantum machine learning with tensor networks*, *Quantum Sci. Technol.* **4**, 024001 (2019).

[40] L. Slattery and B. K. Clark, *Quantum circuits for two-dimensional isometric tensor networks*, *arXiv:2108.02792* (2021).

[41] M. D. Reed, B. R. Johnson, A. A. Houck, L. DiCarlo, J. M. Chow, D. I. Schuster, L. Frunzio, and R. J. Schoelkopf, *Fast reset and suppressing spontaneous emission of a superconducting qubit*, *Appl. Phys. Lett.* **96**, 203110 (2010).

[42] P. Magnard, P. Kurpiers, B. Royer, T. Walter, J.-C. Besse, S. Gasparinetti, M. Pechal, J. Heinsoo, S. Storz, A. Blais, and A. Wallraff, *Fast and unconditional all-microwave reset of a superconducting qubit*, *Phys. Rev. Lett.* **121**, 060502 (2018).

[43] D. Egger, M. Werninghaus, M. Ganzhorn, G. Salis, A. Fuhrer, P. Müller, and S. Filipp, *Pulsed reset protocol for fixed-frequency superconducting qubits*, *Phys. Rev. Applied* **10**, 044030 (2018).

[44] P. Schindler, J. T. Barreiro, T. Monz, V. Nebendahl, D. Nigg, M. Chwalla, M. Hennrich, and R. Blatt, *Experimental repetitive quantum error correction*, *Science* **332**, 1059 (2011).

[45] J. P. Gaebler, C. H. Baldwin, S. A. Moses, J. M. Dreiling, C. Figgatt, M. Foss-Feig, D. Hayes, and J. M. Pino, *Suppression of midcircuit measurement crosstalk errors with micromotion*, *Phys. Rev. A* **104**, 062440 (2021).

[46] N. Khaneja and S. Glaser, *Cartan decomposition of  $SU(2^n)$ , constructive controllability of spin systems and universal quantum computing*, *arXiv:quant-ph/0010100* (2000).

[47] B. Kraus and J. I. Cirac, *Optimal creation of entanglement using a two-qubit gate*, *Phys. Rev. A* **63**, 062309 (2001).

[48] J. Zhang, J. Vala, S. Sastry, and K. B. Whaley, *Geometric theory of nonlocal two-qubit operations*, *Phys. Rev. A* **67**, 042313 (2003).

[49] A. A. Belavin, A. M. Polyakov, and A. B. Zamolodchikov, *Infinite conformal symmetry in two-dimensional quantum field theory*, *Nucl. Phys. B* **241**, 333 (1984).

[50] P. Di Francesco, P. Mathieu, and D. Senechal, *Conformal Field Theory* (Springer, New York, 1997).

[51] J. des Cloizeaux and M. Gaudin, *Anisotropic linear magnetic chain*, *J. Math. Phys.* **7**, 1384 (1966).

[52] J. D. Johnson and B. M. McCoy, *Low-temperature thermodynamics of the  $|\Delta| \geq 1$  Heisenberg-Ising ring*, *Phys. Rev. A* **6**, 1613 (1972).

[53] H.-J. Mikeska and A. K. Kolezhuk, in *Quantum Magnetism*, Vol. 645 of *Lecture Notes in Physics*, edited by U. Schollwöck, J. Richter, D. J. J. Farnell, and R. F. Bishop (Springer, Berlin, 2004), pp. 1–83.

[54] H. A. Bethe, *Zur Theorie der Metalle. I. Eigenwerte und Eigenfunktionen der linearen Atomkette*, *Z. Phys.* **71**, 205 (1931).

[55] V. Korepin, N. Bogoliubov, and A. Izergin, *Quantum Inverse Scattering Method and Correlation Functions* (Cambridge University Press, Cambridge, 1993).

[56] C. N. Yang and C. P. Yang, *One-dimensional chain of anisotropic spin-spin interactions. I. Proof of Bethe's hypothesis for ground state in a finite system*, *Phys. Rev.* **150**, 321 (1966).

[57] C. N. Yang and C. P. Yang, *One-dimensional chain of anisotropic spin-spin interactions. II. Properties of the ground-state energy per lattice site for an infinite system*, *Phys. Rev.* **150**, 327 (1966).

[58] L. Hulthén, *Über das Austauschproblem eines Kristalles*, *Arkiv Mat. Astron. Fys.* **26A**, 1 (1938).

[59] G. V. Uimin, *One-dimensional problem for  $S = 1$  with modified antiferromagnetic Hamiltonian*, *JETP Lett.* **12**, 225 (1970).

[60] C. K. Lai, *Lattice gas with nearest-neighbor interaction in one dimension with arbitrary statistics*, *J. Math. Phys.* **15**, 1675 (1974).

[61] B. Sutherland, *Model for a multicomponent quantum system*, *Phys. Rev. B* **12**, 3795 (1975).

[62] L. A. Takhtajan, *The picture of low-lying excitations in the isotropic Heisenberg chain of arbitrary spins*, *Phys. Lett. A* **87**, 479 (1982).

[63] H. Babujian, *Exact solution of the one-dimensional isotropic Heisenberg chain with arbitrary spins  $S$* , *Phys. Lett. A* **90**, 479 (1982).

[64] H. Babujian, *Exact solution of the isotropic Heisenberg chain with arbitrary spins: Thermodynamics of the model*, *Nucl. Phys. B* **215**, 317 (1983).

[65] A. Läuchli, G. Schmid, and S. Trebst, *Spin nematics correlations in bilinear-biquadratic  $S = 1$  spin chains*, *Phys. Rev. B* **74**, 144426 (2006).

[66] M. Binder and T. Barthel, *Low-energy physics of isotropic spin-1 chains in the critical and Haldane phases*, *Phys. Rev. B* **102**, 014447 (2020).

[67] F. C. Alcaraz and M. J. Martins, *Conformal invariance and critical exponents of the Takhtajan-Babujian models*, *J. Phys. A: Math. Gen.* **21**, 4397 (1988).

[68] H. J. Schulz, *Phase diagrams and correlation exponents for quantum spin chains of arbitrary spin quantum number*, *Phys. Rev. B* **34**, 6372 (1986).

[69] I. Affleck and F. D. M. Haldane, *Critical theory of quantum spin chains*, *Phys. Rev. B* **36**, 5291 (1987).

[70] K. Hallberg, X. Q. G. Wang, P. Horsch, and A. Moreo, *Critical behavior of the  $S = 3/2$  antiferromagnetic Heisenberg chain*, *Phys. Rev. Lett.* **76**, 4955 (1996).

[71] J. Lou, S. Qin, T.-K. Ng, and Z. Su, *Topological effects in short antiferromagnetic Heisenberg chains*, *Phys. Rev. B* **65**, 104401 (2002).

[72] F. B. Ramos and J. C. Xavier, *N-leg spin-S Heisenberg ladders: A density-matrix renormalization group study*, *Phys. Rev. B* **89**, 094424 (2014).

[73] F. D. M. Haldane, *Continuum dynamics of the 1-D Heisenberg antiferromagnet: Identification with the  $O(3)$  nonlinear sigma model*, *Phys. Lett. A* **93**, 464 (1983).

[74] F. D. M. Haldane, *Nonlinear field theory of large-spin Heisenberg antiferromagnets: Semiclassically quantized solitons of the one-dimensional easy-axis Néel state*, *Phys. Rev. Lett.* **50**, 1153 (1983).

[75] H. J. Schulz and T. Ziman, *Finite-length calculations of  $\eta$  and phase diagrams of quantum spin chains*, *Phys. Rev. B* **33**, 6545 (1986).

[76] F. C. Alcaraz and A. Moreo, *Critical behavior of anisotropic spin-S Heisenberg chains*, *Phys. Rev. B* **46**, 2896 (1992).

[77] J. C. Xavier, *Entanglement entropy, conformal invariance, and the critical behavior of the anisotropic spin-S Heisenberg chains: DMRG study*, *Phys. Rev. B* **81**, 224404 (2010).

[78] M. Dalmonte, E. Ercolessi, and L. Taddia, *Critical properties and Rényi entropies of the spin- $\frac{3}{2}$  XXZ chain*, *Phys. Rev. B* **85**, 165112 (2012).

[79] Y.-Y. Shi, L.-M. Duan, and G. Vidal, *Classical simulation of quantum many-body systems with a tree tensor network*, *Phys. Rev. A* **74**, 022320 (2006).

[80] V. Murg, F. Verstraete, O. Legeza, and R. M. Noack, *Simulating strongly correlated quantum systems with tree tensor networks*, *Phys. Rev. B* **82**, 205105 (2010).

[81] As discussed in Ref. [102], one can also increase the number of parameters by iteratively increasing number of Trotter steps  $t$ .

[82] J. R. McClean, S. Boixo, V. N. Smelyanskiy, R. Babbush, and H. Neven, *Barren plateaus in quantum neural network training landscapes*, *Nat. Commun.* **9**, 4812 (2018).

[83] M. Cerezo, A. Sone, T. Volkoff, L. Cincio, and P. J. Coles, *Cost function dependent barren plateaus in shallow parametrized quantum circuits*, *Nat. Commun.* **12**, 1791 (2021).

[84] Q. Miao and T. Barthel, *Absence of barren plateaus for isometric tensor network states*, to be submitted (2023).

[85] T. Barthel and Q. Miao, *Absence of barren plateaus and scaling of gradients in the energy optimization of isometric tensor network states*, to be submitted (2023).

[86] W. Huang, K. A. Gallivan, and P.-A. Absil, *A Broyden class of quasi-Newton methods for Riemannian optimization*, *SIAM Journal on Optimization* **25**, 1660 (2015).

[87] M. Hauru, M. Van Damme, and J. Haegeman, *Riemannian optimization of isometric tensor networks*, *SciPost Phys.* **10**, (2021).

[88] I. A. Luchnikov, M. E. Krechetov, and S. N. Filippov, *Riemannian geometry and automatic differentiation for optimization problems of quantum physics and quantum technologies*, *New J. Phys.* **23**, 073006 (2021).

[89] E. Knill, G. Ortiz, and R. D. Somma, *Optimal quantum measurements of expectation values of observables*, *Phys. Rev. A* **75**, 012328 (2007).

[90] D. Wang, O. Higgott, and S. Brierley, *Accelerated variational quantum eigensolver*, *Phys. Rev. Lett.* **122**, 140504 (2019).

[91] In the QAE scheme, it is not feasible to use mid-circuit qubit resets. Hence, the number of qubits required for TMERA is then not system-size independent but grows (at most) logarithmically in the system size. Still, only the causal-cone qubits need to reside in the quantum register and the others can be moved to a quantum memory [10].

[92] G. Evenbly and G. Vidal, *Quantum criticality with the multi-scale entanglement renormalization ansatz*, *arXiv:1109.5334* (2011).

[93] L. Cincio, J. Dziarmaga, and M. M. Rams, *Multi-scale entanglement renormalization ansatz in two dimensions: quantum Ising model*, *Phys. Rev. Lett.* **100**, 240603 (2008).

[94] G. Evenbly and G. Vidal, *Entanglement renormalization in two spatial dimensions*, *Phys. Rev. Lett.* **102**, 180406 (2009).

[95] A. Luther and I. Peschel, *Calculation of critical exponents in two dimensions from quantum field theory in one dimension*, *Phys. Rev. B* **12**, 3908 (1975).

[96] P. Calabrese, M. Campostrini, F. Essler, and B. Nienhuis, *Parity effects in the scaling of block entanglement in gapless spin chains*, *Phys. Rev. Lett.* **104**, 095701 (2010).

[97] K. Wright, K. M. Beck, S. Debnath, and al., *Benchmarking an 11-qubit quantum computer*, *Nat. Commun.* **10**, (2019).

[98] N. M. Linke, D. Maslov, M. Roetteler, S. Debnath, C. Figgatt, K. A. Landsman, K. Wright, and C. Monroe, *Experimental comparison of two quantum computing architectures*, *Proc. Natl. Acad. Sci. U.S.A.* **114**, 3305 (2017).

[99] D. J. Wales and J. P. Doye, *Global optimization by basin-hopping and the lowest energy structures of Lennard-Jones clusters containing up to 110 atoms*, *J. Phys. Chem. A* **101**, 5111 (1997).

[100] J. Stokes, J. Izaac, N. Killoran, and G. Carleo, *Quantum natural gradient*, *Quantum* **4**, 269 (2020).

[101] D. Wierichs, C. Gogolin, and M. Kastoryano, *Avoiding local minima in variational quantum eigensolvers with the natural gradient optimizer*, *Phys. Rev. Research* **2**, 043246 (2020).

[102] R. Haghshenas, J. Gray, A. C. Potter, and G. K.-L. Chan, *Variational power of quantum circuit tensor networks*, *Phys. Rev. X* **12**, 011047 (2022).